Supplementary Information

Cu–N Coordination–Mediated H_2S Absorption and Controlled Oxidation for Efficient Wet Oxidative Desulfurization

*Zhihao Liu[1], Renji Zheng[2], Zhijie Chen[3] **

[1] College of Environmental and Ecology, Chongqing University, Shapingba District, 401331 Chongqing, China

[2] School of Minerals Processing and Bioengineering, Central South University, Changsha 410083, China

[3] School of Civil and Environmental Engineering, The University of New South Wales, Sydney, NSW 2052, Australia

Corresponding Author: Zhijie Chen

Email: zhijie.chen1@unsw.edu.au

Text S1. Materials and Instruments

N,N-Dimethylformamide (DMF, analytical grade), Tianjin Damao Chemical Reagent Factory, China; Anhydrous copper chloride (analytical grade), Chengdu Kelong Chemicals Co., Ltd., China; 1-Methylimidazole (analytical grade), Shanghai Macklin Biochemical Technology Co., Ltd., China; H_2S standard gas (0.53% H_2S, balanced with N2), Chongqing Lituo Gas Co., Ltd., China; Oxygen (99.5% purity), Chongqing Lituo Gas Co., Ltd., China. Fourier transform infrared spectrometer (ThermoNicolet iS5), Thermo Fisher Scientific, USA; Thermogravimetric analyzer (NETZSCH TG 209F3), Netzsch Analyzing & Testing Instruments (Shanghai) Co., Ltd., China; X-ray photoelectron spectrometer (Thermofisher Escalab 250Xi), Thermo Fisher Scientific, USA; X-ray diffractometer (Ultima IV), Rigaku Corporation, Japan; Hydrogen sulfide detector (PGM-2680), Honeywell International Inc., USA.

Text S2.Computational details

All density functional theory (DFT) calculations in this study were performed using the Gaussian software package [1]. Specifically, theoretical calculations were carried out with Gaussian 09 [2], employing the B3LYP functional together with the 6-311++G(d,p) basis set [3] for both geometry optimization and single-point energy calculations. In addition, the SMD solvation model [4] was applied in evaluating the binding energies of the Cu-N configurations. Molecular models of Cu-N and Cu-N-HS complexes were constructed, and their structures were optimized followed by single-point energy calculations. By comparing the relative binding energies under identical conditions, the most stable molecular structure was identified. Furthermore, DFT calculations were used to investigate the dissociation energy changes of the Cu-N-HS complex in the presence of O_2, thereby confirming the feasibility of the regeneration process observed in the desulfurization experiments [5]. Calculation of molecular configuration binding energy Ebinding: $E_{binding}=E_{Cu\text{-}N}-E_{Cu}-E_{defeact}$,Among them, $E_{Cu\text{-}N}$,E_{Cu} and $E_{defeact}$ refer to the energy of Cu-N coordination product, Cu^{2+} and Cu-free catalyst respectively.

Text S3.Metal corrosion test

Following the NACE RP-0775-91 corrosion standard, 304 and 316L stainless-steel coupons were used for corrosion testing. The coupons were pretreated as follows: they were successively ground with abrasive paper to a smooth finish to remove the surface oxide layer; ultrasonically cleaned in ethanol and deionized water for 10 min each to remove grease; then degreased/descaled, dried, and weighed. Both types of coupons were immersed in the desulfurization solution at room temperature under two exposure configurations—full immersion and half immersion. The solution was renewed every 168 h. After 30 d of exposure, the coupons were removed, rinsed repeatedly with ethanol and deionized water, dried, and reweighed.The average corrosion rate was calculated according to:

$$V = \frac{k(w_1 - w_2)}{Fty}$$

where V is the average corrosion rate ($mm.a^{-1}$); $k=8.76\times10^4$; W_1 and W_2 are the coupon masses before and after exposure (g); F is the exposed surface area (25 cm^2); t is the exposure time (720 h); and y is the density of the coupon material ($g.cm^{-3}$).

Text S4. Techno-Economic Analysis

The cost estimation of the H_2S conversion process using different solvent formulations was conducted according to the following assumptions. In this study, the existing facilities of the conventional Lo-CAT process were adopted, assuming identical equipment purchase and capital investment costs; therefore, only the operating expenditure (OPEX) was analyzed. For the cost evaluation, the system was assumed to operate for 7200 hours per year (300 days), with a gas treatment capacity of 2160 m^3/d. The inlet H_2S concentration was set at 5000 ppm (representing a high-sulfur condition), and the target outlet concentration was 20 ppm, corresponding to an H_2S removal efficiency of approximately 99.6%. Under these conditions, the annual H_2S removal amount was estimated to be about 118.2 tons, equivalent to approximately 111.2 tons of elemental sulfur produced. The benchmark electricity price for Chinese enterprises in 2025 was taken as ¥0.794/kWh (GlobalPetrolPrices), which is within the same order

of magnitude as the provincial average industrial electricity tariff reported by the Chinese Society for Electrical Engineering (0.36–0.67 ¥/kWh). Based on these parameters, a comparative analysis with the conventional Lo-CAT process was subsequently performed, followed by a detailed OPEX evaluation.

The ionic liquid prices used in this study were obtained from commercial supplier quotations and published literature: For [BMIM][$FeCl_4$], the unit cost was taken from IOLITEC Ionic Liquids Technologies GmbH (Germany) and Sigma-Aldrich 2024–2025 catalogues, listed at approximately 500 EUR.kg^{-1}. Using an exchange rate of 7.8 RMB EUR^{-1}, this corresponds to ≈ 3900 RMB kg^{-1}. This range agrees well with recent reports of laboratory-scale Fe-based ionic liquids (≈ 4000 – 5000 RMB.kg^{-1}).For $[P_{66614}]_2[CuCl_4]$, the cost was adopted from Aminuddin et al., *Ind. Eng. Chem. Res.*, 2025, 64, 13489–13511, which cited the Sigma-Aldrich Malaysia purchasing price of ≈ 15000 RM kg^{-1}, equivalent to ≈ 23000 RMB kg^{-1} (1 RM = 1.56 RMB). Similar trihexyl(tetradecyl)phosphonium-based ionic liquids are priced at 20000–25000 RMB.kg^{-1} in the IoLiTec and Sigma-Aldrich catalogues, confirming the representativeness of this value.All quoted prices correspond to laboratory-grade (≥ 95% purity) materials, reflecting small-scale synthesis costs. Although industrial-scale production could reduce prices by 50–70%, the present techno-economic analysis adopts these laboratory values to maintain consistency with the referenced TEA methodology.

1. Unified calculation boundary and general parameters

Parameter	Value / Description
Gas flow rate	2160 $Nm^3.h^{-1}$
H_2S concentration	5000 ppmv (inlet); ≤ 20 ppmv (outlet), removal efficiency ≈ 99.6%
Annual operating time	7200 $h \cdot y^{-1}$ (300 days × 24 h)

Parameter	Value / Description
Annual H_2S removal	($m_{H_2S,y} = 481 \times 34.08 / 1000 \times 7200 = 1.182 \times 10^5$) $kg.y^{-1}$
Air requirement for oxidation	Theoretical O_2 = 0.5 $mol.mol^{-1}$ H_2S; 2×stoichiometric→51.2 $Nm^3 \cdot h^{-1}$
Industrial electricity price (China)	0.52 $RMB.kWh^{-1}$(CSEE, 2024; typical range 0.36–0.68 $RMB \cdot kWh^{-3}$)
Solvent make-up assumption	1% per year under dry-gas conditions (higher for $[P_{66614}]$/DMF due to moisture sensitivity)
Initial solvent inventory	1.5 m^3 (uniform for all systems)

Physical properties and unit prices

System	Density ($kg \cdot L^{-1}$)	Viscosity (mPa·s, 25°C)	Characteristics	Unit price ($RMB \cdot kg^{-1}$)	Source
Cu–1-MI/DMF	0.944	0.8–0.9	Low viscosity, non-scaling, no O_2 in absorber	DMF 20; 1-MI 100; $CuCl_2$ 60	Eastman TDS; Alibaba & 100PPI (Oct 2025)
$[P_{66614}]_2[CuCl_4]$/DMF (1:1 v/v)	1.05	≈ 12	No O_2 in absorber; O_2 in regenerator; Cu^{2+}/Cu^{+} redox; moisture-sensitive	IL 23 000; DMF 20	Aminuddin et al., 2025; Sigma-Aldrich catalog (2024)
[BMIM][$FeCl_4$]	1.359	43	Continuous aeration (absorption + oxidation); sulfur slurry circulation	3900	IOLITEC TDS 2023; 100PPI 2025-10

3. Power consumption

(1) Aeration power

Typical specific aeration energy: 0.015–0.024 kWh·Nm^{-3} air (EPA, 2020).

Cu–MI/DMF and $[P_{66614}]_2[CuCl_4]$/DMF (1:1 v/v) require air only during regeneration → **0.01 kWh·Nm^{-3}**.

Fe-IL requires continuous air supply → **0.02 kWh·Nm^{-3}**.

$$E_{blower}=(\text{Specific energy})\times V_{air}$$

→ 0.512 kWh.h^{-1} (Cu–MI/DMF and $[P_{66614}]_2[CuCl_4]$/DMF (1:1 v/v), 1.024 kWh·h^{-1} (Fe-IL).

(2) Circulation pump power

Based on viscosity ranking: Cu–MI/DMF < $[P_{66614}]_2[CuCl_4]$/DMF (1:1 v/v) < Fe-IL → **4, 6, 15 kW**, respectively.

(3) Annual electricity cost

2. $E_y=(E_{blower}+P_{pump})\times 7200$; $C_e=E_y\times 0.52$

System	**(E_{blower})** **(kWh.h^{-1})**	**(P_{pump})** **(kW)**	**Annual energy** **(kWh.y^{-1})**	**Electric cost** **(RMB.y^{-1})**
Cu–1-MI/DMF	0.512	4	32 486	16 893
$[P_{66614}]_2[CuCl_4]$/DMF	0.512	6	47 686	24 797
[BMIM][$FeCl_4$]	1.024	15	115 373	59 994

4. Initial charge and annual solvent loss

Initial inventory (1.5 m^3 = 1500 L)

System	ρ (kg·L^{-1})	Mass (kg)	Unit price (RMB.kg^{-1})	Initial charge (RMB)
Cu–MI/DMF	0.944	1416	see formulation	3.15×10^4
$[P_{66614}]$/DMF (1:1 v/v)	1.05	1575	(930×23 000 + 708×20)/1638 kg	$\approx 2.14 \times 10^7$
[BMIM][$FeCl_4$]	1.359	2039	3900	7.95×10^6

Annual solvent loss (1 %.y^{-1} under dry-gas conditions)

$$C_{loss}=m\times0.01\times P_{solv}$$

System	Annual loss (RMB·y^{-1})	Remarks
Cu–MI/DMF	1360	Includes DMF (1.2%), 1-MI (1%), $CuCl_2$ (0.1%)
$[P_{66614}]$/DMF (1:1 v/v)	2.14×10^5	High IL price; hydrolysis to HCl possible in humid gas
[BMIM][$FeCl_4$]	7.95×10^4	Hydrolysis to $Fe(OH)_3$ under moist conditions

Note: All cost/economic data above are converted to USD at **1 USD = RMB 7.12.**

Data sources and cost assumptions

All physical property and cost parameters used in the present techno-economic evaluation were obtained from publicly available technical data sheets, industrial market quotations, and authoritative engineering references to ensure traceability and reproducibility.

Eastman Chemical Company. *Dimethylformamide (DMF) – Product Technical Data Sheet.* Eastman Chemical, 2024.
Available at: https://www.eastman.com (Used for solvent viscosity 0.802–0.92 mPa·s at 25 °C and density 0.944 kg·L^{-1}.)

IOLITEC Ionic Liquids Technologies GmbH. *[BMIM][FeCl$_4$] – Technical Data Sheet and Safety Data Sheet.* Heilbronn, Germany, 2023.
Available at: https://www.iolitec.de
(Provides density 1.359 kg·L^{-1}, viscosity 43 mPa·s at 25 °C, and "immiscible with / decomposes in water.")

Merichem Technologies. *LO-CAT® Hydrogen Sulfide Removal Process – Technical Overview.* Houston, TX, 2025.
Available at: https://www.merichem.com/technologies/lo-cat
(Defines LO-CAT as an aqueous, ambient-temperature iron chelate oxidation process.)

Oil & Gas Journal (OGJ). *Operating Costs of Small and Medium Redox Processes for H_2S Removal. Oil & Gas Journal*, Vol. 109, No. 14, 2012, pp. 54–60.
(Provides the benchmark LO-CAT chemical cost ≈ 300 USD · tS^{-1} for small to medium redox systems.)

Merichem Technologies (2025). *Economic and Operating Data for LO-CAT® Units.*
Available at: https://www.merichem.com
(Specifies updated unit operating cost 0.40–0.50 USD · lbS^{-1} ≈ 880–1100 USD · tS^{-1}.)

Gas Processing Association of Canada. *Technical Guidelines for Sulfur Recovery and Redox Processes.* Calgary, AB, 2022.

(Confirms LO-CAT process type, normal operation, and cost scaling.)

China Society for Electrical Engineering (CSEE). *National Industrial Electricity Tariff Statistics (2024 Edition).*

Available at: https://www.csee.org.cn

(Reports typical provincial large-industrial electricity rates 0.36–0.68 RMB · kWh^{-1}; baseline 0.52 RMB · kWh^{-1} adopted.)

U.S. Environmental Protection Agency (EPA). *Wastewater Treatment Design Manual: Fine Bubble Aeration Systems.* EPA/625/1-86/018, 2020 Revision.

(Used for the standard range of specific aeration energy 0.015–0.024 kWh · Nm^{-3}-air.)

Perry, R. H., & Green, D. W. *Perry's Chemical Engineers' Handbook,* 9th Edition. McGraw–Hill, New York, 2019.

(Source for friction factor correlations and hydrodynamic principles, $f_D \propto \mu$ in laminar flow and viscosity effect in transitional regime.)

Kian Resin Co., Ltd. *Dimethylformamide Physical Properties Summary Sheet.*

Available at: https://www.kianresin.com

(Confirms DMF viscosity, boiling point, and safety data consistent with Eastman TDS.)

Chinese Chemical Market Network. *Market Price Data for $FeCl_3$, NaOH, and NTA (2025-10).*

Available at: https://www.100ppi.com

(Used for $FeCl_3$ ≈ 2833 RMB·t^{-1}, NaOH ≈ 3500 RMB·t^{-1}, and NTA ≈ 27 300 RMB·t^{-1} quotations for cost calculations.)

Gas Processing Association of Canada (GPAC). *Processing and Treating Sour Gas: Practical Design Manual.* Calgary, AB, 2023.

(Confirms the engineering boundary conditions and typical air flow/oxidation stoichiometry for H_2S removal systems.)

Supporting Figures

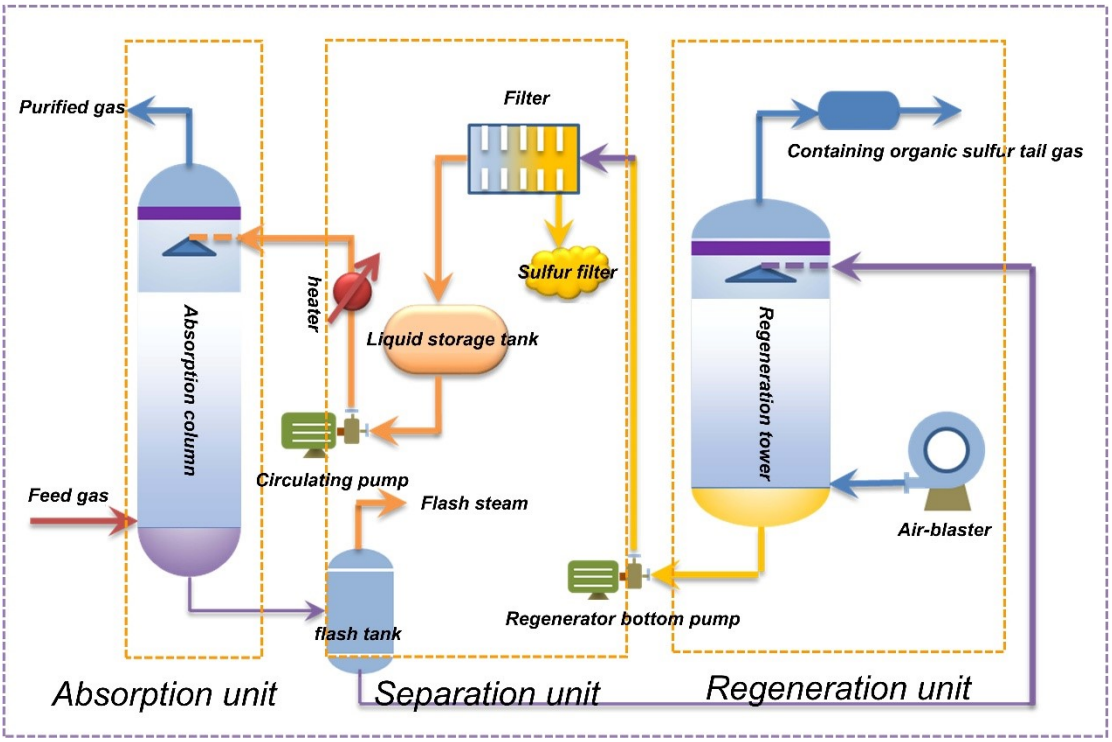

Fig. S1 Classic Lo-cat process.

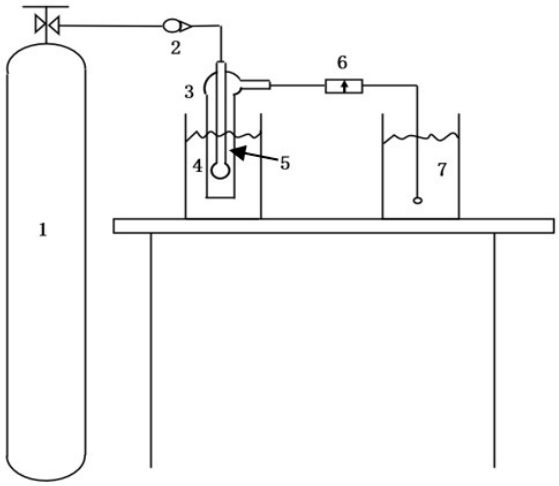

Fig. S2 Schematic Diagram of the Desulfurization Experimental Setup

1.H_2S gas cylinder, 2. Gas flow meter, 3. Bubble reactor, 4. Thermostatic water bath, 5. Desulfurizer, 6. H_2S detector, 7. Saturated sodium hydroxide solution.

.

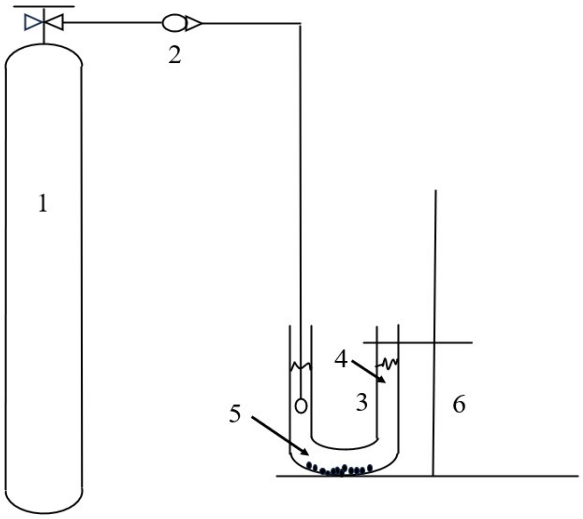

Fig. S3 Simple Device Diagram of Regeneration Experiment.

1. Oxygen cylinder, 2. Gas flowmeter, 3.U-shaped tube, 4. Desulfurization rich liquid, 5. Solid product, 6. Iron frame.

4.

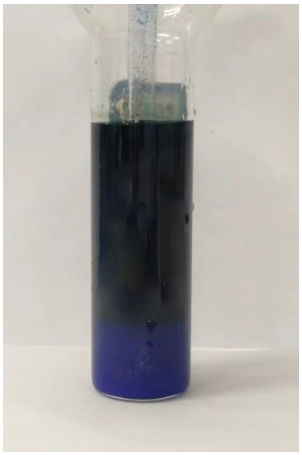

Fig. S4 Desulfurization liquid appearance.

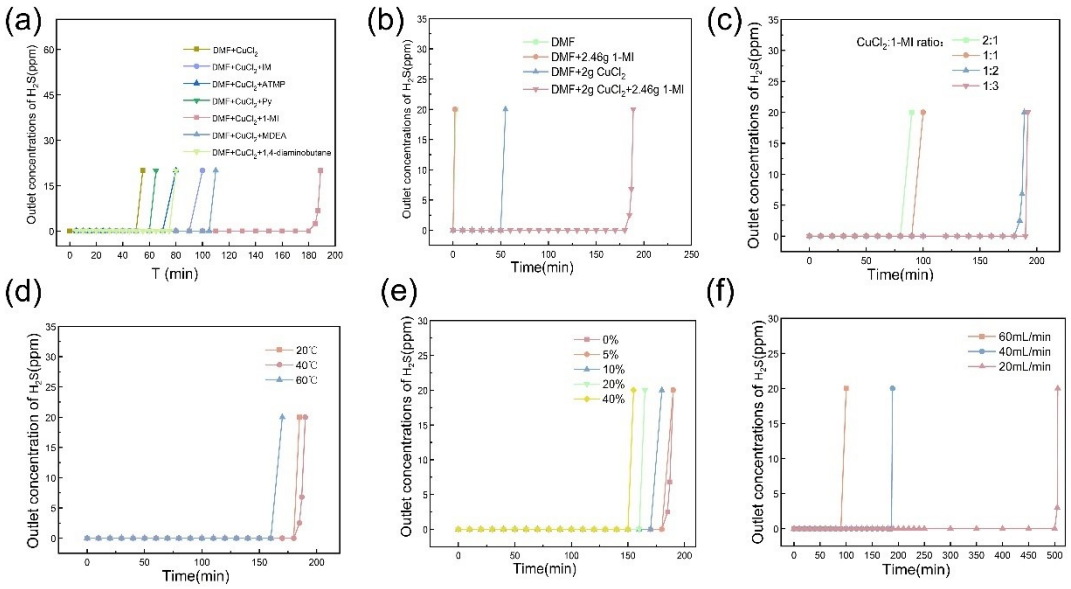

Fig. S5 Breakthrough curves of desulfurization solutions under different components and reaction conditions; (a) type of ligands, (b) composition of the solution, (c) ratio of Cu to 1-MI, (d) reaction temperature, (e) moisture content, and (f) gas flow rate.

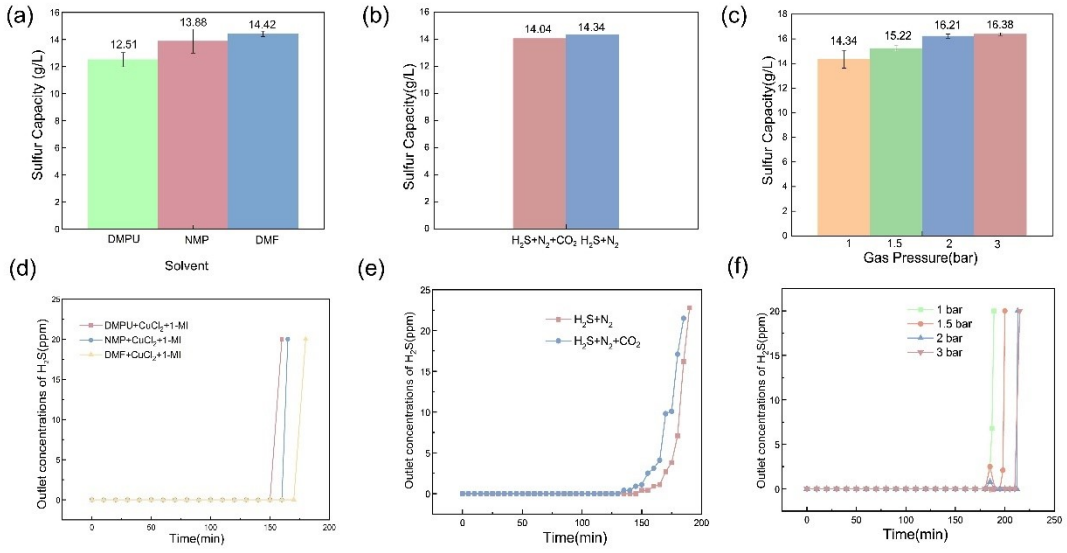

Fig. S6 Breakthrough curves and sulfur capacity of desulfurization solutions under different components and reaction; (a,d) type of solvent, (b,e) gas flow selectivity, and (c,f) gas pressure.

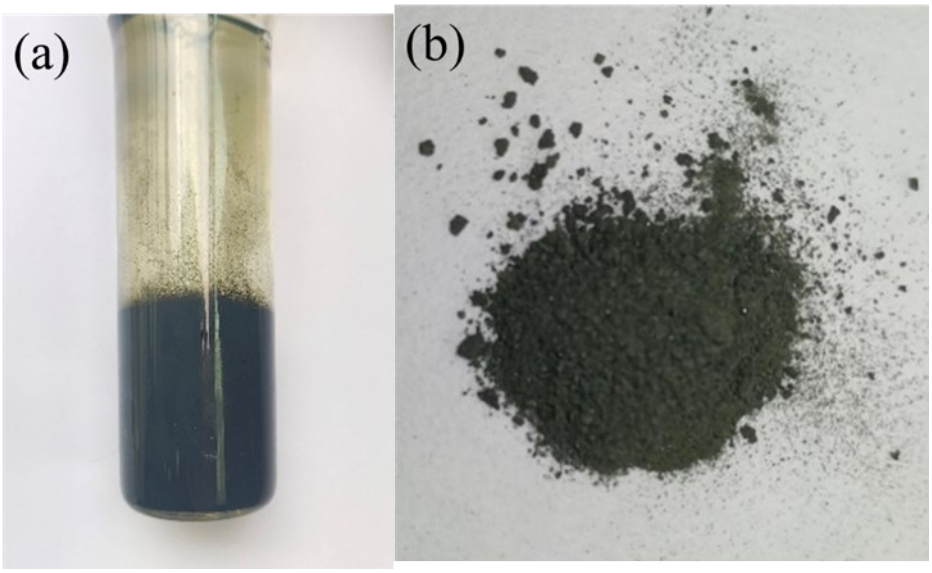

Fig. S7 Appearance of desulfurization solution after desulfurization and separated solids.

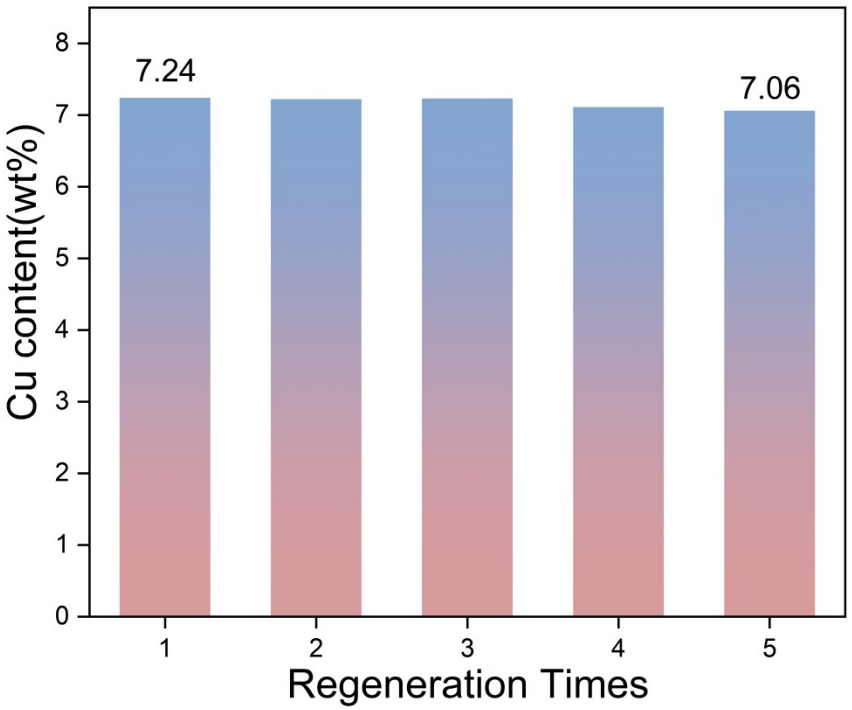

Fig.S8 The Cu content in the desulfurization liquid detected by ICP-OES.

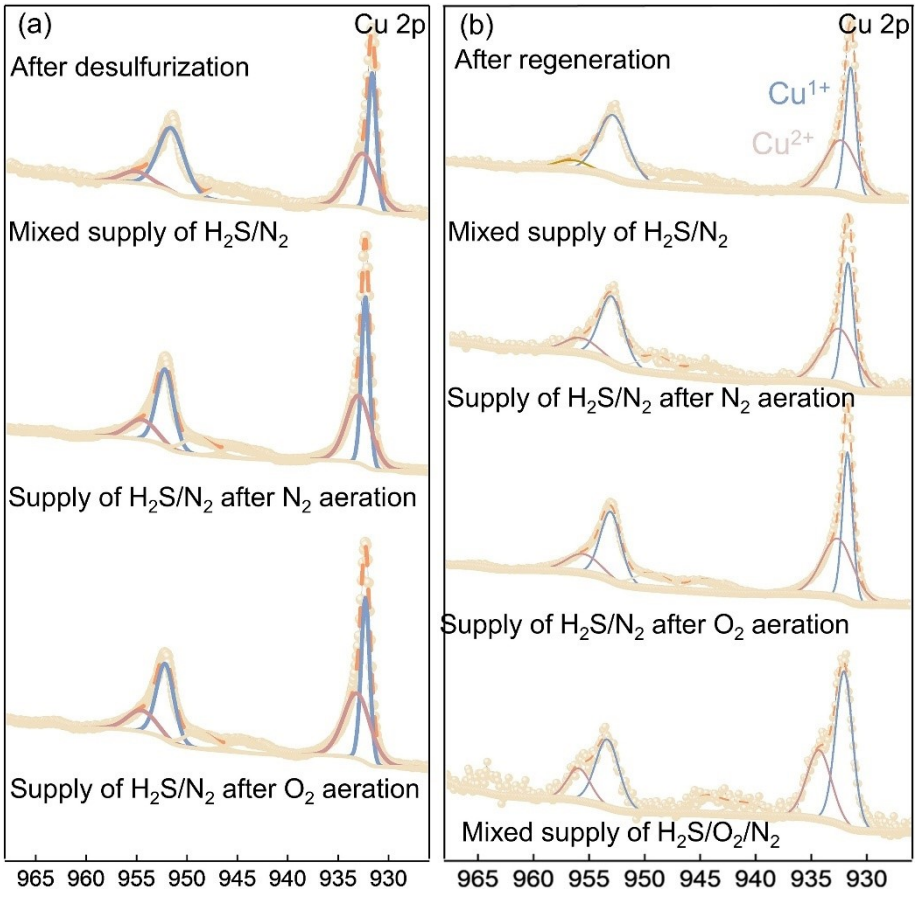

Fig. S9 The XPS fine spectra of the Cu2p orbitals in solid samples at different stages.

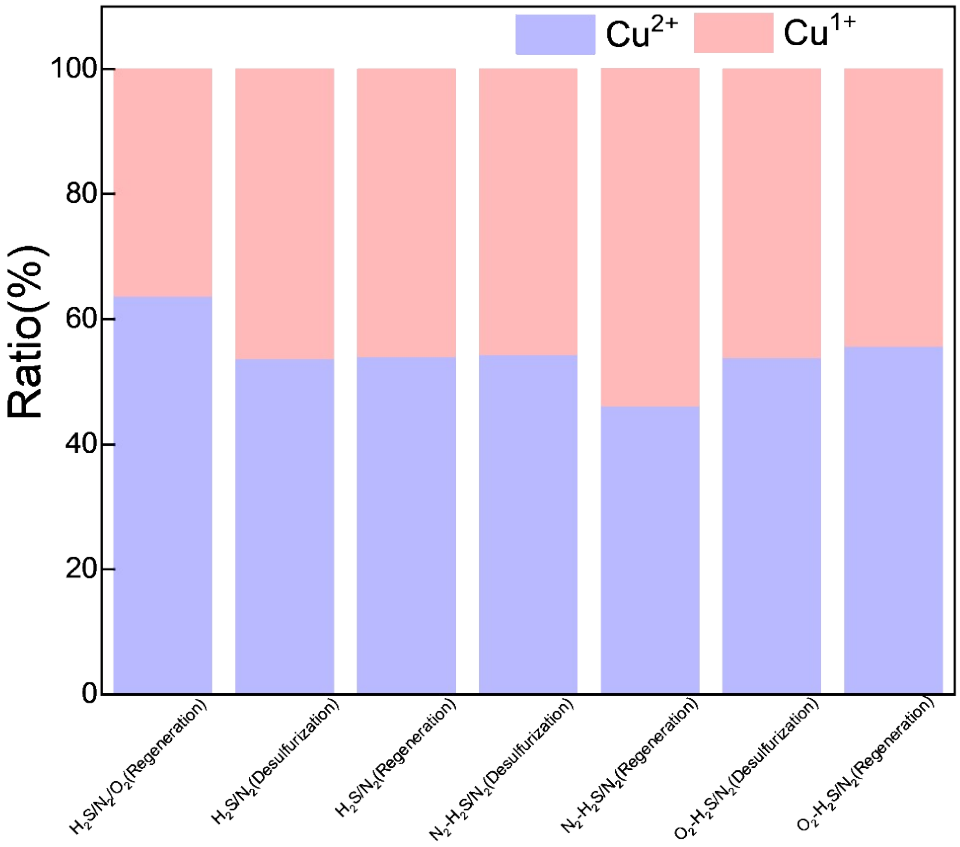

Fig. S10 The proportion of Cu species obtained through quantitative peak analysis using XPS.

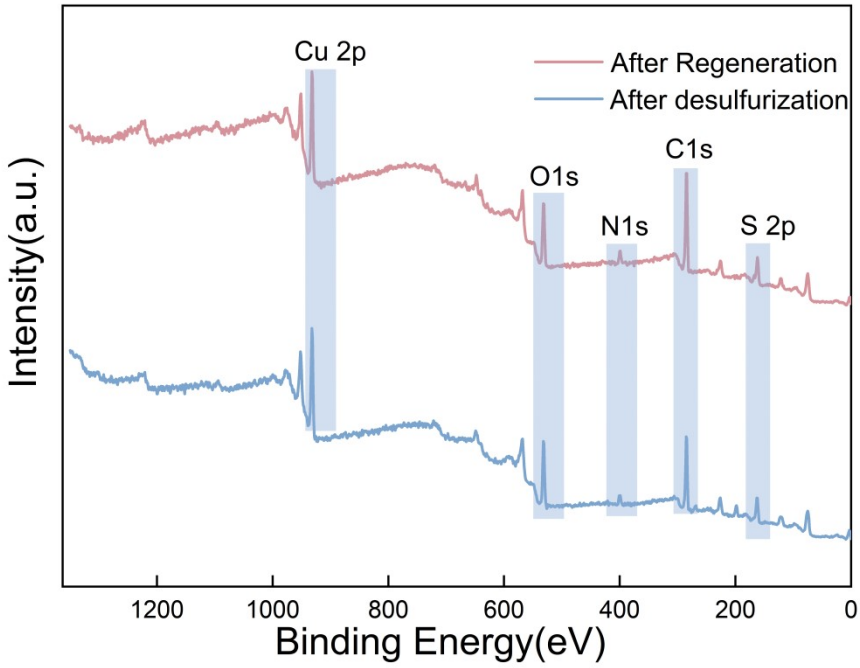

Fig. S11 XPS full spectrum of solid samples was obtained after desulfurization and regeneration.

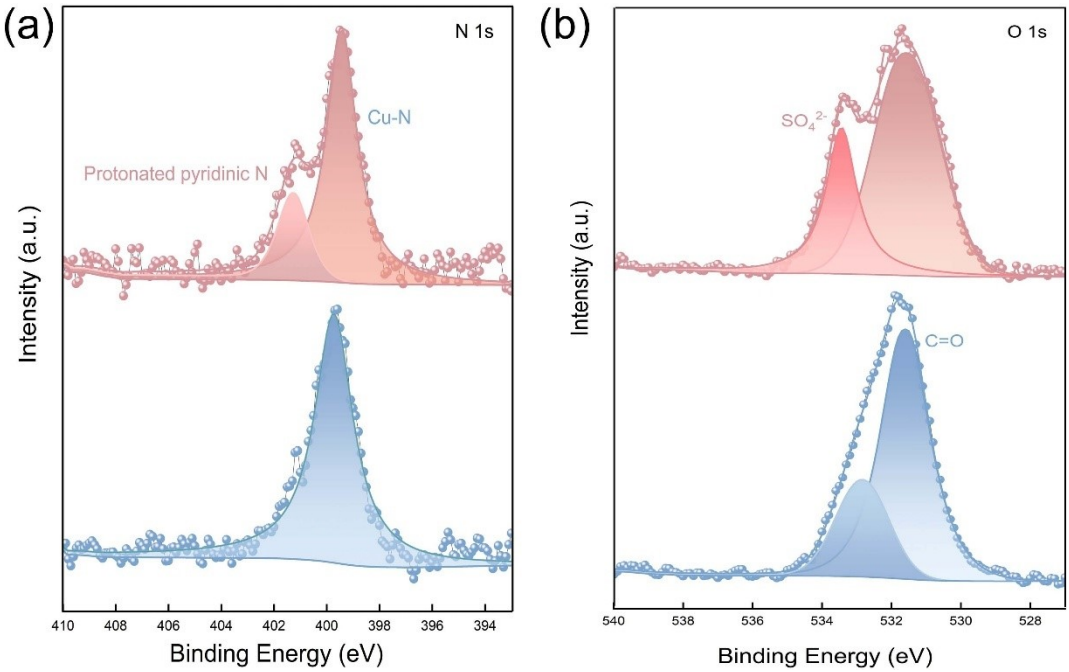

Fig. S12 The XPS fine spectra of the N 1S,O1S orbitals in solid samples at different stages.

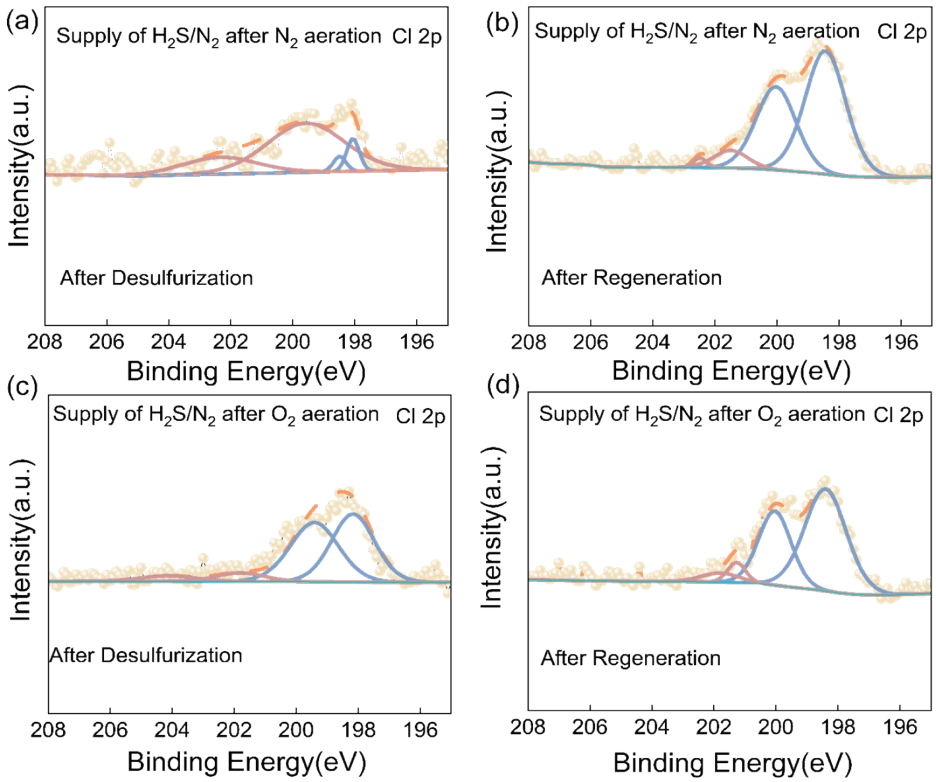

Fig. S13The XPS fine spectra of the Cl 2p orbitals in solid samples at different stages.

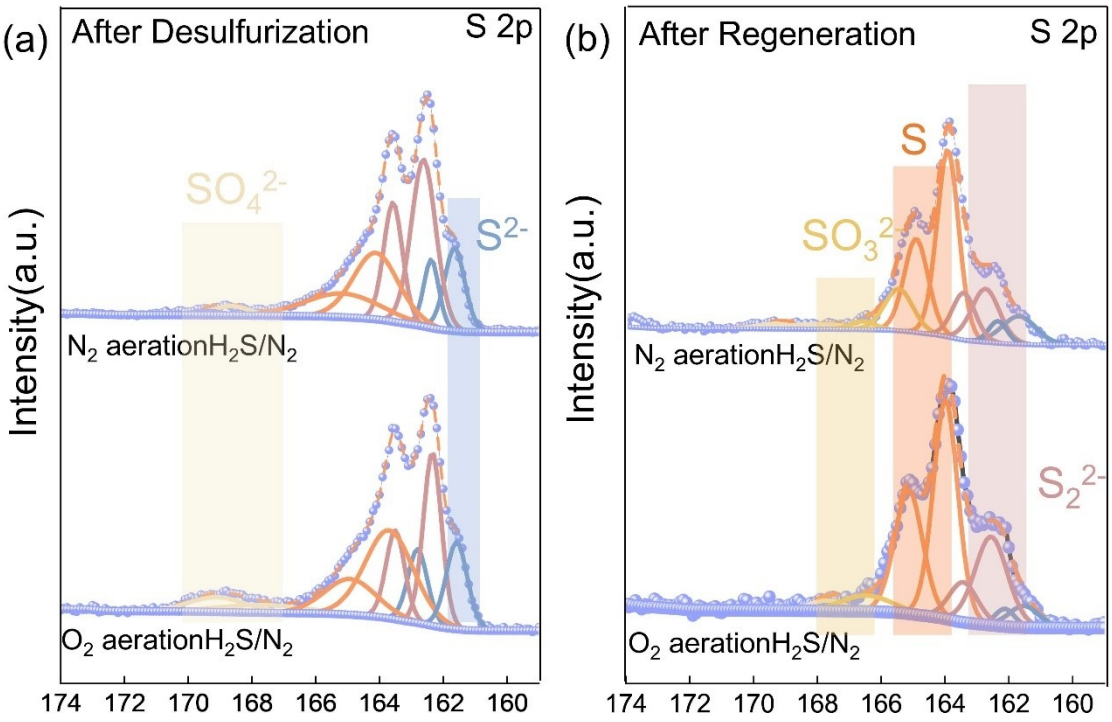

Fig. S14 The detailed XPS spectra of the S 2p orbitals in solid samples at different stages, as well as the semi-quantitative determination of the proportions of each species.

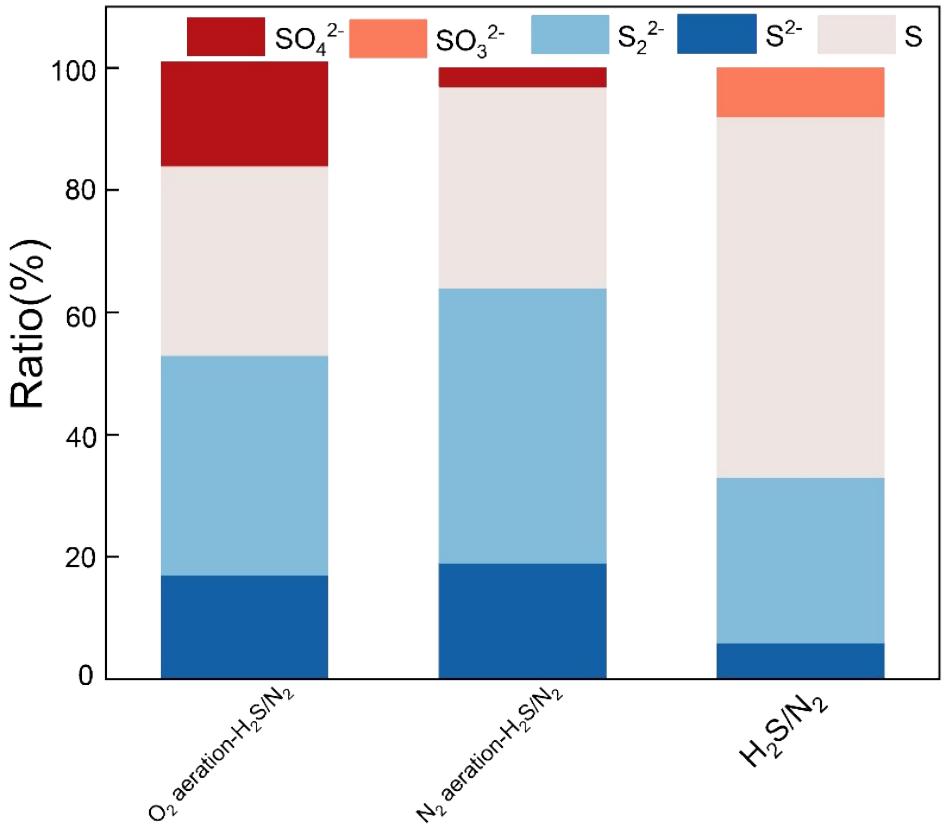

Fig. S15 The detailed XPS spectra of the S 2p orbitals in solid samples at different stages, as well as the semi-quantitative determination of the proportions of each species.

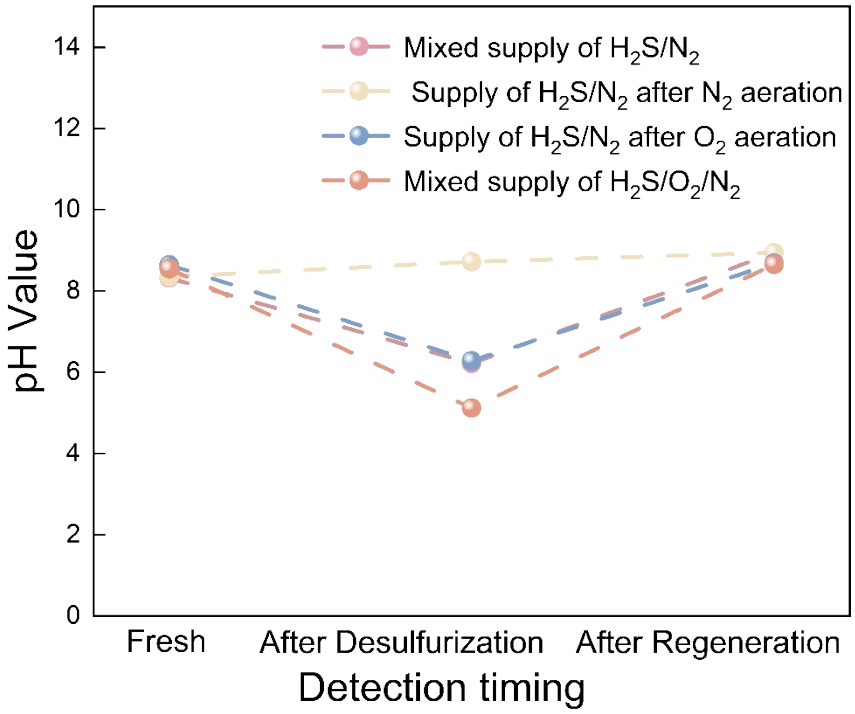

Fig. S16 Changes in dissolved oxygen and pH in the desulfurization solution under different operating conditions.

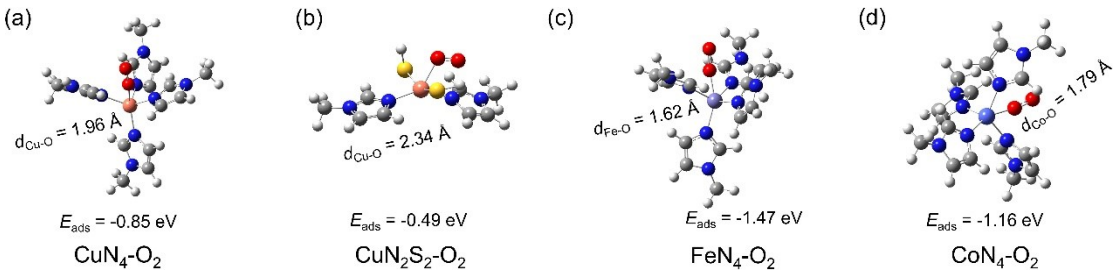

Fig. S17 The adsorption energy of oxygen for different molecular configurations.

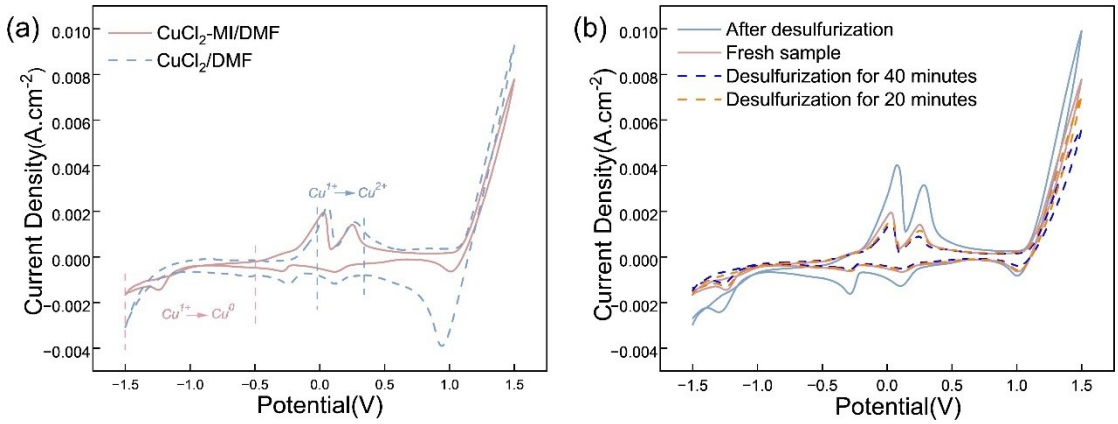

Fig. S18 Cyclic voltammograms of the desulfurization solutions at each stage.

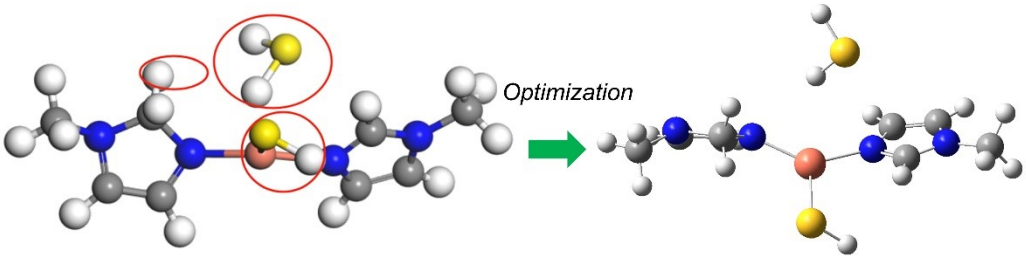

Fig. S19 Schematic diagram of spontaneous dehydrogenation of adsorbed H_2S molecules.

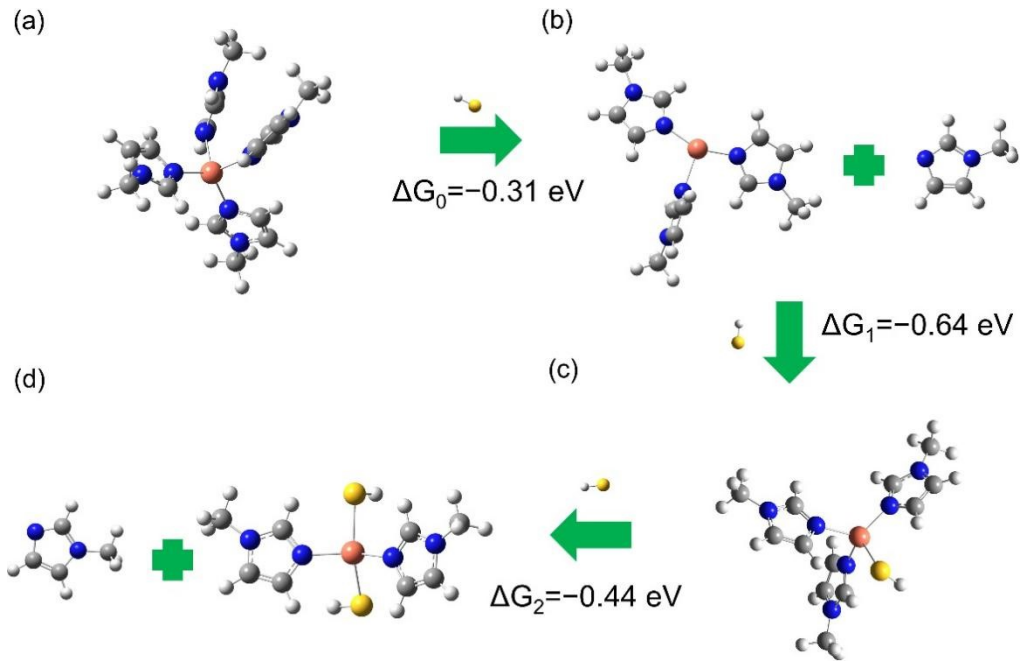

Fig. S20 The Gibbs free energy for the transformation of the CuN_4 configuration to the CuN_2S_2 configuration in the DMF solution.

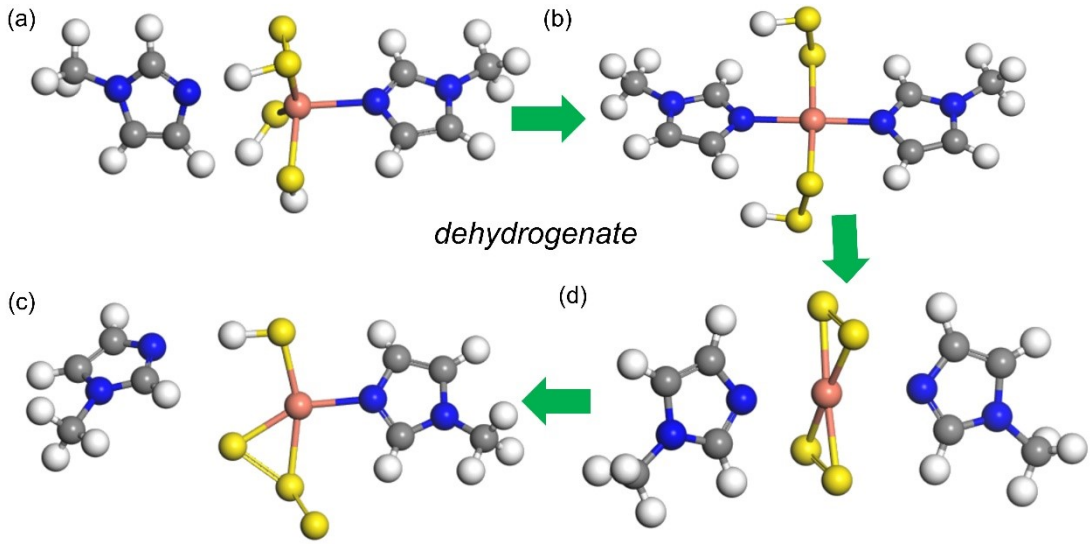

Fig. S21 Schematic diagram of sulfur step polymerization step anchored at Cu-N site under the action of oxygen.

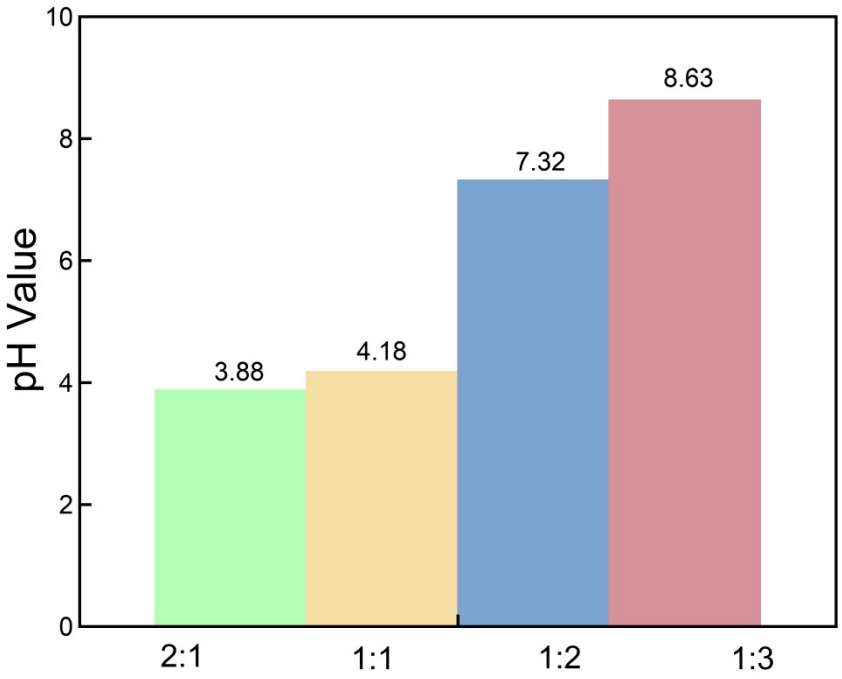

Fig. S22 pH value of liquids with different Cu: methylimidazole ratios.

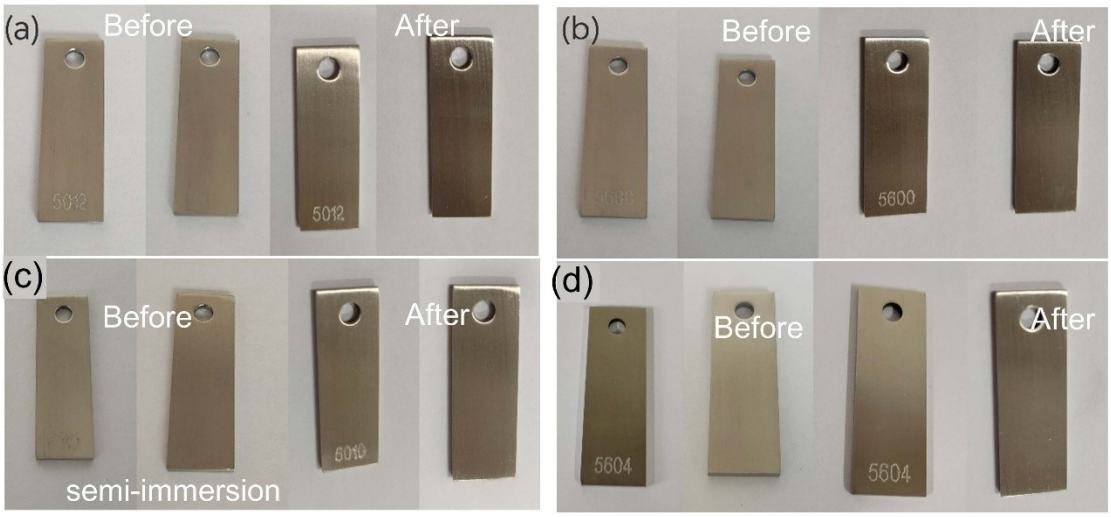

Fig. S23 After the immersion corrosion test in Cu-MI/DMF solution (0 % H_2O), the appearance photos of the stainless steel plate were taken.

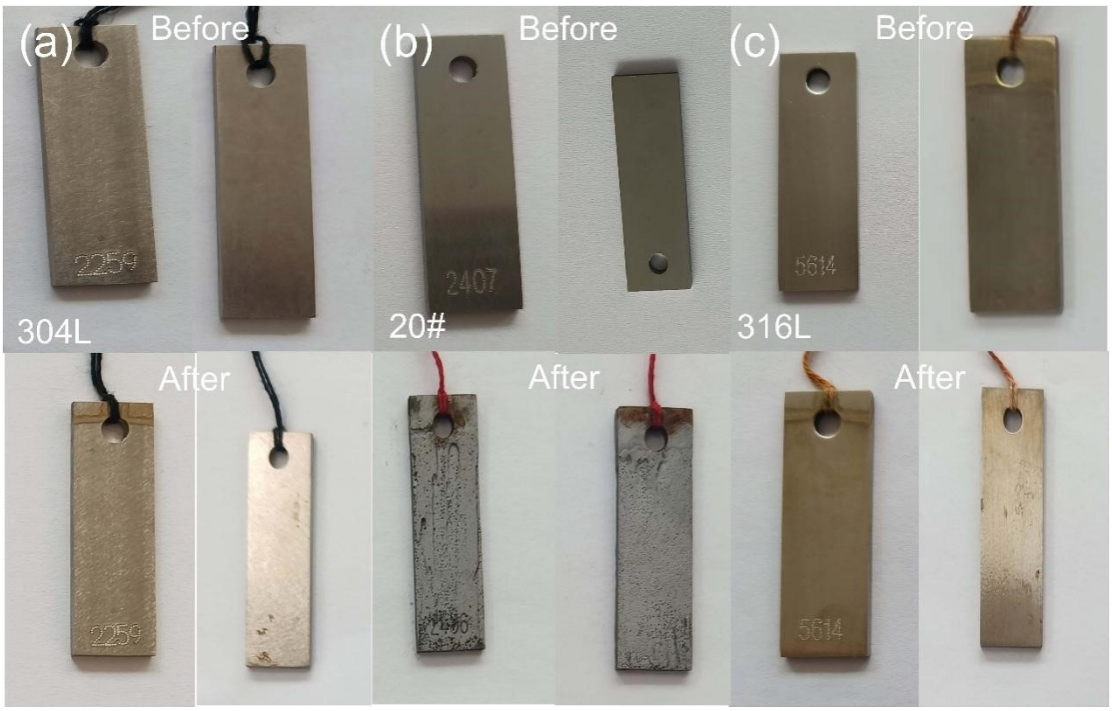

Fig. S24 After the immersion corrosion test in Cu-MI/DMF solution (5% H_2O), the appearance photos of the stainless steel plate were taken.

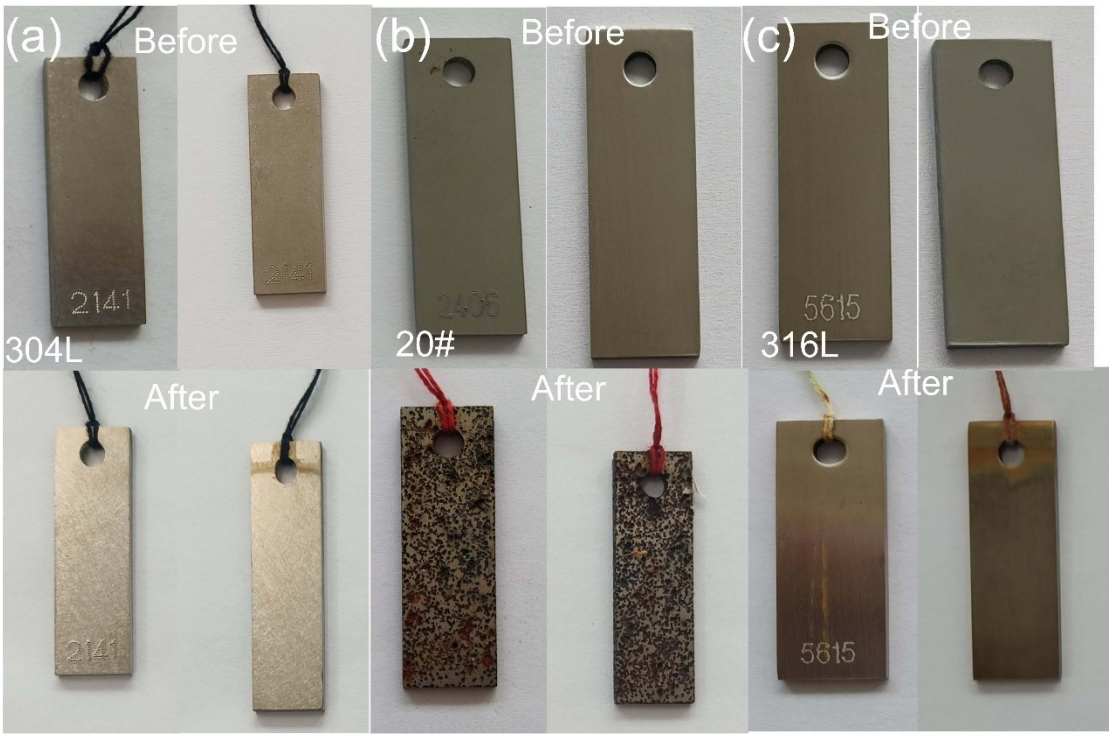

Fig. S25 After the immersion corrosion test in Cu-MI/DMF solution (10% H_2O), the appearance photos of the stainless steel plate were taken.

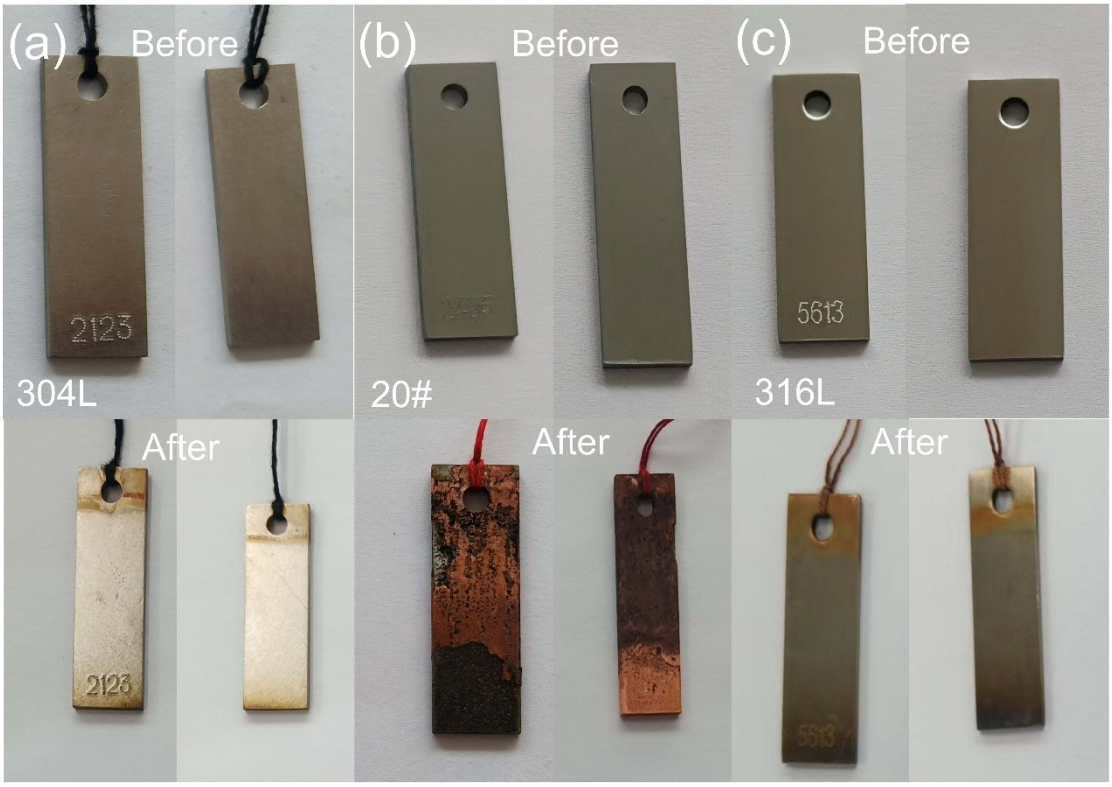

Fig. S26 After the immersion corrosion test in Cu-MI/DMF solution (20% H_2O), the appearance photos of the stainless steel plate were taken.

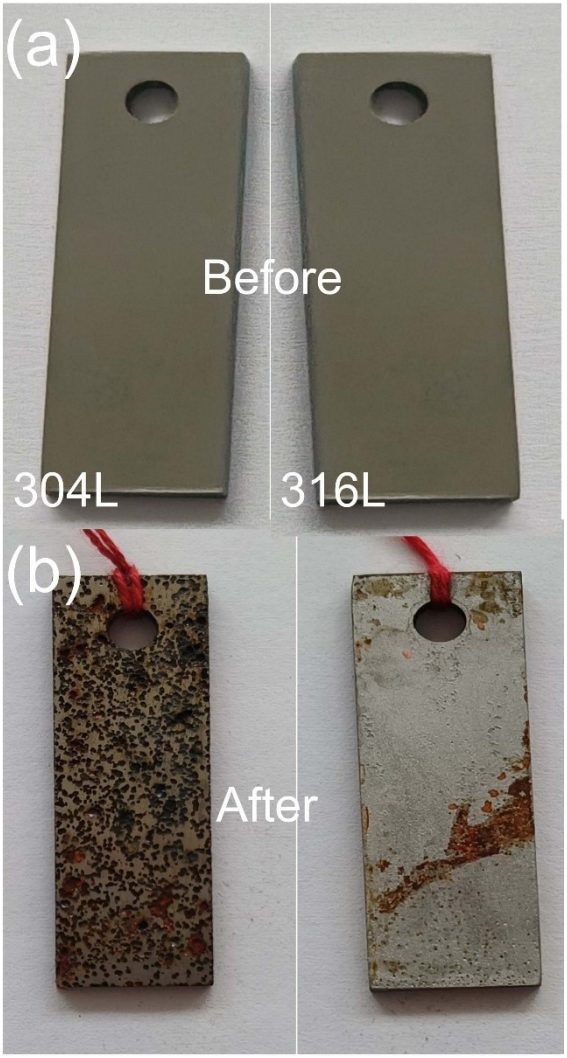

Fig. S27 After continuous air supply in Cu-MI/DMF solution for 21 days, an immersion corrosion test was conducted on the stainless steel plate. The appearance photos of the stainless steel plate were taken.

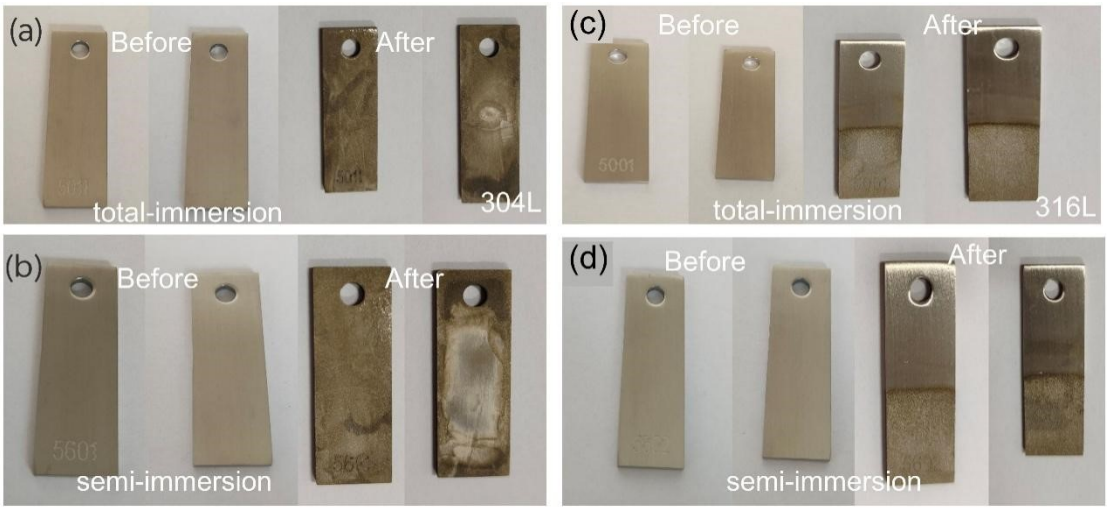

Fig. S28 Appearance photos of stainless steel sheet after immersion corrosion test in Cu-DMF system.

Supporting Tables

Table S1 Density determination of desulfurizers at different temperatures and ratios

Temperature/ K	ρ_1 (g/cm^3)	ρ_2 (g/cm^3)	ρ_3 (g/cm^3)	ρ_4 (g/cm^3)
293.15	0.9842	0.9948	1.0944	1.0847
313.15	0.9849	0.9946	1.0941	1.0840
333.15	0.9778	0.9945	1.0947	1.0836

Note: ρ_1, Cu^{2+}: 1-MI = 2:1; ρ_2, Cu^{2+}: 1-MI = 1:1; ρ_3, Cu^{2+}: 1-MI = 1:2; ρ, Cu^{2+}: 1-MI = 1:3.

Table S2 Measurement of viscosity of desulfurizers at different temperatures and Cu^{2+}: 1-MI ratios

Temperature /K	η_1 (mPa·s)	η_2 (mPa·s)	η_3 (mPa·s)	η_4 (mPa·s)
293.15	3.00	4.00	4.20	-
313.15	2.95	3.92	4.05	-
333.15	2.80	3.75	3.98	-

Note: η_1, Cu^{2+}: 1-MI = 2:1; η_2, Cu^{2+}: 1-MI = 1:1; η_3, Cu^{2+}: 1-MI = 1:2; η_4, Cu^{2+}: 1-MI = 1:3.

Table S3 Three times desulfurization-regeneration experiment of desulfurizer with different solvent components

	DMPU	NMP	DMF
The first desulfurization time /min	160	165	180
The second desulfurization time /min	156	150	170
The third desulfurization time /min	135	140	160

Table S4 Metal specimen corrosion table (Cu-1-IM/DMF) No additional water was added

texture	Operation	Pre-reaction weight (g)	After-reaction weight (g)	Density (g/m^3)	Average corrosion rate (mm/a)
304	Semi-immersion	7.7833	7.7828	7.92	0.0003
316L	Semi-immersion	7.9076	7.9074	8.03	0.0001
304	Total immersion	7.8034	7.8014	7.92	0.0012
316L	Total immersion	7.9564	7.9553	8.03	0.0007

Table S5 Metal specimen corrosion table (Cu-DMF)

texture	Operation	Pre-reaction weight (g)	After-reaction weight (g)	Density (g/m^3)	Average corrosion rate (mm/a)
304	Semi-immersion	7.7756	7.3490	7.92	0.2621
316L	Semi-immersion	7.9221	7.5956	8.03	0.1979
304	Total immersion	7.8004	7.5799	7.92	0.1355
316L	Total immersion	7.9118	7.7146	8.03	0.1195

Table S6 Metal specimen corrosion table (Cu-1-MI/DMF in 5% H_2O)

texture	Operation	Pre-reaction weight (g)	After-reaction weight (g)	density (g/m^3)	Average corrosion rate (mm/a)
20#	Total immersion	8.4885	6.5445	7.85	1.7217
304	Total immersion	7.6356	7.6315	7.92	0.0036
316L	Total immersion	7.9425	7.9395	8.03	0.0026

Note: The immersion corrosion test period lasts for 28 days. During this period, the appearance of the metal sheet is observed and its weight is measured every 7 days.

Table S7 Metal specimen corrosion table (Cu-1-MI/DMF in 10% H_2O)

texture	Operation	Pre-reaction weight (g)	After-reaction weight (g)	density (g/m^3)	Average corrosion rate (mm/a)
20#	Total immersion	8.4839	6.9299	7.85	1.3763
304	Total immersion	7.8458	7.8402	7.92	0.0048
316L	Total immersion	7.645	7.6438	8.03	0.0011

Table S8 Metal specimen corrosion table (Cu-1-MI/DMF in 20% H_2O)

Texture	Operation	Pre-reaction weight (g)	After-reaction weight (g)	density (g/m^3)	Average corrosion rate (mm/a)
20#	Total immersion	8.5976	7.4161	7.85	1.046
304	Total immersion	7.9534	7.9478	7.92	0.0048
316L	Total immersion	7.6638	7.6601	8.03	0.0032

Table S9 Comparison of operating costs between the Cu-MI/DMF system and the H_2S removal system based on the IL approach

System	Annual electricity bill (USD/y)	Chemical replenishment (USD /y)	OPEX (USD /y)	Initial inventory (USD /y)	USD/1000 Nm^3	USD /kg-H_2S
Cu-MI/DMF	2372	191	2.56×10^3	4412	0.163	0.022
$BMIMFeCl_4$	8426	1.12×10^4	1.95×10^4	3.05×10^6	1.247	0.284
$[P_{66614}]_2[CuCl_4]$/DMF	3482.72	3.01×10^4	3.36×10^4	1.11×10^6	2.139	0.166

Table S10 EDS results of solid particles

Element	Atom fraction(%)
S	98.35
Cu	1.55
Total	100.00

Table S11 Formation energy of each intermediate configuration after Gaussian optimization

Path way	$E_{binding\ energy}$ (eV)
Cu+2*Methylimidazole→ Cu-2-Methylimidazole	-0.50
Cu-2-Methylimidazole+2HS→Cu-2-Methylimidazole-2HS	-5.82
Cu-2-Methylimidazole+4HS→Cu-2-Methylimidazole-4HS	-6.29
Cu-2-Methylimidazole-2HS→Cu-2-Methylimidazole-HS-S + H	2.07
Cu-2-Methylimidazole-2HS +0.25*O_2→Cu-2-Methylimidazole-HS-S + 0.5*H_2O	0.37
Cu-2-Methylimidazole-HS-S +0.25*O_2→Cu-2-Methylimidazole-S-S + 0.5*H_2O	-0.77
Cu-3-Methylimidazole+HS→Cu-3-Methylimidazole-HS	-3.79

Suppoerting references

[1] Gaussian 09, Revision D.01, M. J. Frisch, G. W. Trucks, H. B. Schlegel, G. E. Scuseria, M. A. Robb, J. R. Cheeseman, G. Scalmani, V. Barone, B. Mennucci, G. A. Petersson, H. Nakatsuji, M. Caricato, X. Li, H. P. Hratchian, A. F. Izmaylov, J. Bloino, G. Zheng, J. L. Sonnenberg, M. Hada, M. Ehara, K. Toyota, R. Fukuda, J. Hasegawa, M. Ishida, T. Nakajima, Y. Honda, O. Kitao, H. Nakai, T. Vreven, J. A. Montgomery, Jr., J. E. Peralta, F. Ogliaro, M. Bearpark, J. J. Heyd, E. Brothers, K. N. Kudin, V. N. Staroverov, T. Keith, R. Kobayashi, J. Normand, K. Raghavachari, A. Rendell, J. C. Burant, S. S. Iyengar, J. Tomasi, M. Cossi, N. Rega, J. M. Millam, M. Klene, J. E. Knox, J. B. Cross, V. Bakken, C. Adamo, J. Jaramillo, R. Gomperts, R. E. Stratmann, O. Yazyev, A. J. Austin, R. Cammi, C. Pomelli, J. W. Ochterski, R. L. Martin, K. Morokuma, V. G. Zakrzewski, G. A. Voth, P. Salvador, J. J. Dannenberg, S. Dapprich, A. D. Daniels, O. Farkas, J. B. Foresman, J. V. Ortiz, J. Cioslowski, and D. J. Fox, Gaussian, Inc., Wallingford CT, 2013.

[2] Frisch M J, Trucks G W, Schlegel H B, et al. Gaussian 09, revision D.01, gaussian, Inc, wallingford CT, 2013.

[3] Dede B, Özen N, Görgülü G. Synthesis, characterization, theoretical calculations and enzymatic activities of novel diimine-dioxime ligand and its homodinuclear Cu (II) complex[J]. Journal of Molecular Structure, 2018, 1163: 357-367.

[4] Marenich A V, Cramer C J, Truhlar D G. Universal solvation model based on solute electron density and on a continuum model of the solvent defined by the bulk dielectric constant and atomic surface tensions[J]. The Journal of Physical Chemistry B, 2009,113(18): 6378-6396.

[5] Lampert H, Mikeenda W, Karpfen A. Molecular Geometries and Vibrational Spectra of Phenol, Benzaldehyde, and Salicyladehyde: Experimental versus Quantum Chemical Data[J]. Journal of Physical Chemistry A, 1977, 101(12): 2254-2263.